applied sciences

MDPI

Article

Application of Fatty Acids Distillation Products as a Substitute for Heavy Fuel Oil in Stationary Combustion Chambers

Janusz Lasek [1,*], Krzysztof Głód [1], Agata Czardybon [1], Yueh-Heng Li [2] and Chao-Wei Huang [3]

[1] Institute of Energy and Fuel Processing Technology, ul. Zamkowa 1, 41-803 Zabrze, Poland; kglod@itpe.pl (K.G.); aczardybon@itpe.pl (A.C.)
[2] Department of Aeronautics and Astronautics, National Cheng Kung University, Tainan City 70101, Taiwan; yueheng@mail.ncku.edu.tw
[3] Department of Engineering Science, National Cheng Kung University, No.1, Daxue Rd., East District, Tainan City 70101, Taiwan; huangcw@nkust.edu.tw
* Correspondence: jlasek@itpe.pl

Featured Application: The application of fatty acids distillation products as fuel allows the substitution of heavy fuel oil and decreases the use of fossil fuels. As a result, it reduces CO_2 emissions, and is a way to obtain sustainable energy transition.

Abstract: Liquid biofuels are of special interest due to the possibility of their application as a substitute for fossil liquid fuels. The necessary step is to investigate the possibility of bio-fuel application in terms of its properties and similarities to fossil liquid fuels (e.g., crude oil, heavy fuel oil, diesel). The properties and combustion performance of heavy fuel oil (HFO) and products of the fatty acids distillation residues (FADR) were analyzed in this study. The application of animal-fat-delivered fuels is fully suggested in the literature. Nevertheless, the investigations focused on the raw materials or their transformation into diesel. The novelty of this paper is the utilization of FADR as a substitute for HFO. The utilization of FADR allows the use of this material as a feedstock to obtain valuable products (fuel) and avoids generating waste after animal fat processing. The experimental investigations were carried out using a technical-scale 150 kW_{th} combustion chamber. FADR can be recognized as a substitute for HFO due to its beneficial calorific properties and viscosity. Other beneficial effects are the significantly lower emission of SO_2 (lower than 1 ppm) and PAHs (i.e., 355 $\mu g/m^3_n$) during the combustion of FADR. Finally, the application of FADR requires less energy demand for fuel heating and pressurization.

Keywords: animal fats; fatty acids; heavy fuel oil; bio-liquids; combustion; NO_x

Citation: Lasek, J.; Głód, K.; Czardybon, A.; Li, Y.-H.; Huang, C.-W. Application of Fatty Acids Distillation Products as a Substitute for Heavy Fuel Oil in Stationary Combustion Chambers. *Appl. Sci.* **2023**, *13*, 13233. https://doi.org/10.3390/app132413233

Academic Editor: Matteo Prussi

Received: 8 November 2023
Revised: 7 December 2023
Accepted: 12 December 2023
Published: 13 December 2023

1. Introduction

The energy system transition to CO_2-neutral requires the change and diversification of energy sources. One of the possible ways is to apply biomass-derived fuels [1]. Within different options, liquid biofuels are of special interest due to their similarities with fuels obtained using crude oil processing [2,3]. According to the definition presented by Kupczyk et al. [4] "liquid biofuels constitute a fuel category, which includes substances made of raw materials of organic origin—biomass or biodegradable fractions of waste" [4]. One considered option is the application of animal waste (e.g., fats) as a feedstock to produce valuable fuels [5]. Another motivation to use this waste as an energy feedstock is the large amount of this material produced per year [6,7]. According to the Statistics Poland Statistical Yearbook of Agriculture [8], in 2020, the production of meat from slaughtered animals was 337,180 thousand tonnes and 5246 thousand tonnes in the world and Poland, respectively. In Poland, the production of fats from slaughter was 403 thousand tonnes in 2021, whereas the consumption of fats from slaughter was 204 thousand tonnes in 2021 (p. 305 in [8]). The production of animal fat not intended for human consumption, AFN, was 1,351,955.3

in EU 27 and 102,279.9 in Poland [9]. It was estimated that biodiesel from animal fat achieves nearly 80% fossil CO_2 reduction compared with 30% for soya [7]. Animal fats are considered a feedstock for biodiesel production [5,7] and different chemical products [6,7]. Rosson et al. [6] listed six groups of potential applications that are related to the specific treatment processes. They mentioned (1) biodiesel production using transesterification, (2) paraffinic fuel production using catalytic cracking, hydrogenation, and isomerization, (3) production of hydrocarbon N-/O-heterocycles using pyrolysis, (4) emulsified biofuel production using microemulsion, (5) blended biofuel production using direct mixing of animal fats, and (6) bioliquid production using direct use and purification process. Brahma and colleagues [10] presented a review paper on biodiesel synthesis from various mixed oils. They discussed (inter alia) different types of reactors for biodiesel synthesis. Animal fat can be used in the process of biodiesel production followed by the distillation process as a key step [5]. There is a common idea that any organic material, specifically carbohydrates, proteins, and fats, could be converted into crude oil [11]. It should be underscored that within animal fat production, some parts of this material cannot be used for food production. They are included in the waste group if a reasonable way of application is not presented. In the literature, this part of the animal part is called the Animal By-products Not Intended for Human Consumption, ABNIHC [12], or animal fat not intended for human consumption, AFN [7]. These materials can be used as a feedstock for fuel production. In such a way, this step is desired in the waste management hierarchy [13]. Namely, the direct application of fat waste as a fuel or its utilization as feedstock in the production of fuels and/or valuable chemicals increases the waste management level from the disposal level to the recovery or recycling level. There are different strategies for waste treatment to obtain valuable products. One of the possible ways is thermo-chemical treatment, including such processes as hydrothermal treatment [11,14], distillation [5], and thermal treatment [3,15].

There are investigations on the application of animal fats as a fuel in stationary combustion chambers. Alonso et al. [9] presented the combustion AFN and co-combustion of AFN with other liquid fuels in a 26.7 kW boiler (fuel consumption 1.86 kg/h). Lezsovits and Könczöl [16] presented the combustion of animal fat using a rotary cup-type burner in a 4 MW_{th} boiler. They compared the results with the combustion of heavy fuel oil. They observed lower NO_x emission (164 ppm referred to as 3 vol% O_2) compared with HFO combustion (295 ppm referred to as 3 vol% O_2). The nitrogen content in animal fat and HFO was 0.35 w.% and 0.3 w.%, respectively. Alonso et al. [12] presented the combustion of Animal By-products Not Intended for Human Consumption (ABNIHC) in a technical-scale combustion chamber. Bondera et al. [17] investigated the combustion of animal fats from bovine and swine mixed with liquid hydrocarbons in a 55 kW boiler. The concentration of animal fat in a mixture was up to 30% by mass. The addition of animal fat caused slightly lower emission of NO_x. Wasielewski and Głód [18] presented the combustion of the fatty acids distillation residues (FADR) and the heavy fuel oil (HFO) in a 4.5 MW_{th} nominal capacity boiler. A slight decrease in NO_x emission and a significant decrease in SO_2 emission were observed. Lazaroiu and colleagues [19] presented the combustion of animal fats and other biofuels (i.e., vegetable oils and solid biomass). Animal fat waste was provided by the leather industry. The experimental tests were carried out using a diesel engine and pilot boiler (Multiplex CL 50 model, manufactured by Thermostahl Company). The blends of diesel and animal fat (10–30% by mass) were applied as a fuel. Very low NO_x emission values, with a mean of 26 ppm, were obtained. Emission of CO was in the range of 920–3640 ppm.

The application of animal-fat-delivered fuels is fully suggested in the literature. Nevertheless, the efforts focused on the application of raw fats or their processing products into biodiesel. The utilization of heavy fractions after fat distillation is poorly reported in the literature. Especially the technical-scale experience of fuel feeding, combustion performance, and emission of gaseous pollutants should be investigated. Thus, this paper aims to fill this knowledge gap. The possibility of heavy fuel oil, HFO, substitution is suspected and fully recommended due to the possibility of CO_2 emission reduction.

2. Materials and Methods

2.1. Material

The heavy fuel oil, HFO, and the products of the fatty acids distillation residues (FADR) were applied as a fuel. FADR was obtained during the processing of the animal fats. In the first step, the fats were filtered in the presence of diatomaceous earth. Next, the material was processed in the hydrolysis reactor at a temperature of 250 °C and a pressure of 55 bar. In this process, there was separation in a glycerol–water solution and the fatty acids were obtained. Next, the fatty acids were distilled and the heavy fraction products (>C18, as c.a. 5–8% by mass of total products) were applied. This material is a viscous, oily substance with a dark color and a peculiar and characteristic smell. The ultimate analysis was performed using a LECO TrueSpec (LECO, St. Joseph, MI, USA) CHN analyzer and a LECO SC 632 analyzer (LECO, USA). The heating value was analyzed using the LECO AC500 (LECO, USA) apparatus. The ignition temperature was determined using the Marcusson method. The liquid fuel sample was placed in an open vessel and it was heated up (rate of 3 °C/minute). The gaseous fuel flame was approaching the liquid fuel sample within the temperature increase of 1 °C until ignition of the liquid fuel volatiles occurred [20,21]. Density was determined using aerometric analysis at a temperature of 60 °C. The viscosity of the liquid fuel sample was determined using an Engler viscometer. The viscosity measurement was conducted at a shearing velocity of 500 1/s.

2.2. Combustion Test

The combustion tests were carried out using a technical-scale combustion chamber (height of 3.4 m and internal diameter of 0.6 m), which was used in previous research [22]. The three main parts of the installation are the combustion chamber with burners, a high-temperature precipitator, and an exhaust gas cooling system. The schematic of the experimental setup is presented in Figure 1. The combustion chamber is equipped with four burners: (1) main burner (gaseous, liquid, or pulverized), (2) additional gaseous burner, (3) pilot burner (gaseous), and (4) radial burner. Burners (1)–(3) are situated at the top cover of the combustion chamber. The radial burner is situated in the cylindrical wall (close to the top zone) of the chamber. The maximum possible liquid fuel feed to the main burner is 14 kg/h. The system of liquid fuel consists of the fuel tank, fuel pipes, valves system, and pump. The temperature of liquid fuel was controlled using heating elements. The maximum possible temperature of liquid fuel is 250 °C. A dust separator (DS) is equipped with ceramic elements. The particles were removed from the DS using pressurized air impulses. The maximal admissible temperature of flue gas in the DS zone is 600 °C. The heating of the combustion chamber was performed using a natural gas burner and the burner was switched to liquid fuel burner. The average natural gas flow rate (during the heating period) was 6.5 m^3/h (input power ~65 kW). The flame structure was observed using an inspection hole (window) placed at the top part of the chamber. The temperature in the combustion zone was measured at three points of the chamber: 958 mm (top zone, TT), 1258 mm (central zone, TC), and 1508 mm (bottom zone, TB) from the top cover of the chamber. The flue gas was continuously analyzed for CO_2 (0–45 v.%), CO (0–6000 ppmv), H_2O (0–30 v.%), NO (0–1000 ppmv), N_2O (0–200 ppmv), NO_2 (0–200 ppmv), SO_2 (0–6000 ppmv), C_4H_{10} (butane; 0–500 ppmv), C_7H_8 (toluene, 0–200 ppmv), CHOH (formaldehyde; 0–50 ppmv) using an FTIR analyzer (GASMET DX4000), and O_2 (inlet and outlet), which was measured using a paramagnetic analyzer (Oxymat 61) and a zirconium sensor analyzer (AMS Analysen). The measurement uncertainty of the presented analyzers was estimated at below 2% of the total measuring range.

As in our previous research [23], PAHs were analyzed using the application of a measurement system, including an externally heated glass filter and a set of tubes, including XAD-2 resin and active carbon. The captured organic matter in the glass filter and tubes were processed using extraction (ASE 350 provided by DIONEX) in the presence of acetone and methylene chloride. Solvents were evaporated using RAPIDVAP apparatus provided by Labconco, and the next TOC was determined. Finally, the quantitative

analysis of 16 PAHs was carried out using a gas chromatograph and a flame ionization detector (Trace-GC provided by Thermo Scientific, Waltham, MA, USA). A total of 16 PAH emissions included the following compounds: naphthalene, acenaphthylene, acenaphthene, fluorene, phenanthrene, anthracene, fluoranthene, pyrene, benzo(a)anthracene, chrysene, benzo (b + k) fluoranthene, benzo(e)pyrene, benzo(a)pyrene, beryline, bibenzo(a, h) anthracene + indeno (1, 2, 3) pyrene, and benzo(g, h, i) perylene.

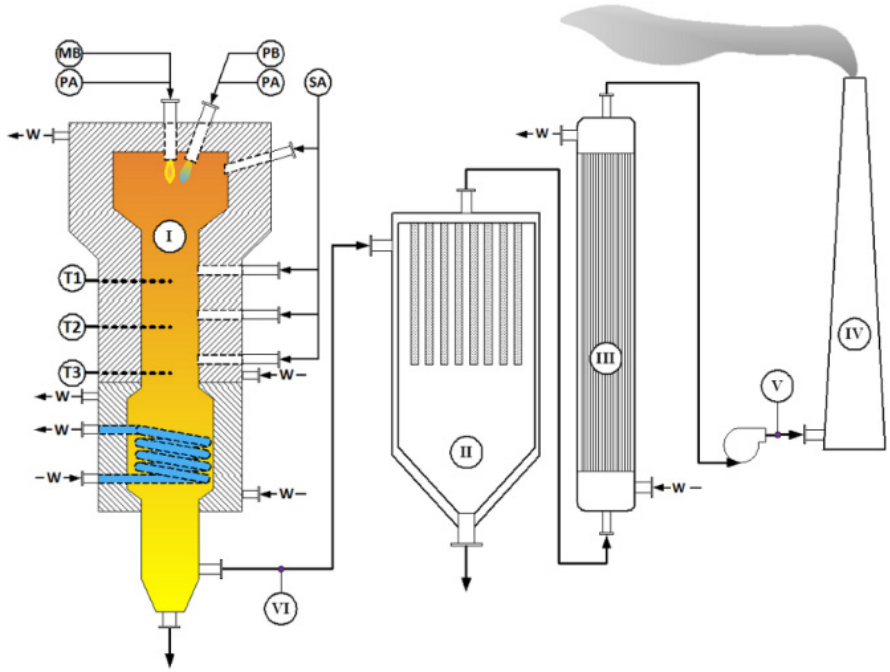

Figure 1. Scheme of a technical-scale installation used for combustion of liquid fuels. MB—main burner (liquid fuels: FADR and HFO), PB—pilot burner (fuel: natural gas), PA—primary air, SA—secondary air, W—water for cooling, I—combustion chamber, II—dust separator, III—exhaust gas cooler, IV—chimney, V—exhaust gas sampling point, VI—O_2 measurement in raw exhaust gas. Reprinted from [24] (upon permission of Elsevier, License Number 5656340853661).

2.3. Uncertainty Analyses

Uncertainty analyses were presented according to the procedure presented in the previous literature [20]. It is known that the relative (ΔA) and the absolute (δA) uncertainty of a considered parameter A are related by Equation (1)

$$\Delta A = (\delta A / A) \times 100\% \tag{1}$$

It can be assumed that for measured parameters A and B, the rules for the uncertainty calculation are described by Equations (2)–(5).

$$(A \pm \delta A) + (B \pm \delta B) \cong (A + B) \pm (\delta A + \delta B), \tag{2}$$

$$(A \pm \delta A) - (B \pm \delta B) \cong (A - B) \pm (\delta A + \delta B), \tag{3}$$

$$(A \pm \Delta A) \times (B \pm \Delta B) \cong (A \times B) \pm (\Delta A + \Delta B), \tag{4}$$

$$(A \pm \Delta A) / (B \pm \Delta B) \cong (A / B) \pm (\Delta A + \Delta B). \tag{5}$$

Moreover, if the final parameter Q is obtained by the multiplication of measured parameter A and number N, $Q = N \times A$, then the absolute uncertainty of Q is described by Equation (6):

$$\delta Q \approx |N| \times \delta A \tag{6}$$

Moreover, if the measured parameter A is changed in time due to stochastic variation (i.e., fluctuation in a certain average value), then the final value of absolute uncertainty of an analyzed parameter, δA, includes the uncertainty related to the measuring system $\delta A_{measuring}$ and the uncertainty related to the measured parameter fluctuation $\delta A_{fluctuations}$. Thus, in such cases, the δA is calculated from Equation (7)

$$\delta A = \sqrt{\delta A_{fluctuations}^2 + \delta A_{measuring}^2} \quad (7)$$

Based on these rules, the uncertainty was calculated from the equations presented below, in terms of the following parameters:

- energy density:

$$\Delta E_{d,\ LHV} = \Delta\rho + \Delta LHV \quad (8)$$

$$\Delta E_{d,\ HHV} = \Delta\rho + \Delta HHV \quad (9)$$

- the energy for fuel heating and fuel pressurization:

$$\Delta E_{heat} = \frac{\delta T_{fuel} + \delta T_{room}}{T_{fuel} - T_{room}} \times 100\% \quad (10)$$

$$\Delta E_{pressur} = \Delta p + \Delta\rho \quad (11)$$

- nominal fuel feed:

$$\Delta\dot{m}_{100\text{kW}} = \Delta LHV \quad (12)$$

- power loss:

$$\Delta P_{loss} = \Delta\dot{m}_{100\text{kW}} + \frac{\delta E_{heat} + \delta E_{pressur}}{E_{heat} + E_{pressur}} \times 100\% \quad (13)$$

The relative and absolute uncertainty of analyzed parameters are presented in Table 1.

Table 1. The relative and the absolute uncertainty of analyzed parameters.

Parameter	FADR		HFO	
	Absolute Uncertainty	**Relative Uncertainty**	**Absolute Uncertainty**	**Relative Uncertainty**
Density, kg/m^3	1	0.11	1	0.1
HHV, kJ/kg	87	0.22	87	0.2
LHV, kJ/kg	120	0.33	120	0.3
C, w.%	1	1.31	1	1.16
H, w.%	0.50	4	0.54	4
N, w.%	0.05	6	0.03	6
S, w.%	0.05	31	0.05	8
Ash content, w.%	0.04	14	0.04	6
Ignition temperature, °C	1	0.4	1	0.4
E $_{density\ (LHV)}$, GJ/m^3	0.142	0.4	0.146	0.4
E $_{density\ (HHV)}$, GJ/m^3	0.155	0.4	0.156	0.4
E_{heat}, kJ/kg	2.85	3	5.13	3
$E_{pressur}$, kJ/kg	10.8	1.8	6.4	1.0
E_{total}, kJ/kg	13.7	1.9	11.5	1.4
P_{loss}, kW	0.044	2.3	0.033	1.7

3. Results and Discussion

3.1. Fuel Properties

The results of the basic properties are presented in Table 2. FADR and HFO have similar properties in terms of calorific value and density. The calorific value (i.e., lower heating value, LHV) of FADR is around 86.7% of the value for HFO. A similar tendency was observed by Xiu et al., who concluded that the higher heating value, HHV, of liquefied oil from swine manure was 36.05 MJ/kg, which is about 90% of that of heavy fuel oil (40 MJ/kg) [11]. Nevertheless, due to the higher density of FADR (i.e., 882 kg/m^3 at 60 °C) compared with HFO (i.e., 864 kg/m^3 at 60 °C), the energy density of FADR (i.e., 32.298 GJ/m^3 (from LHV)) is 88.5% of the value for HFO (i.e., 36.505 GJ/m^3 (from LHV)). The comparison of the energy density (GJ/m^3) based on HHV for different fuels is presented in Figure 2. The value of FADR energy density is similar to the values for diesel, gasoline, micro wax, and crude oil. The lower viscosity of FADR (i.e., at 60 °C 0.0255 Pa·s) was observed compared with HFO (i.e., at 60 °C 0.057 Pa·s). In this case, lower viscosity is an added value in terms of lower energy demand on the compression. It is known that there is a recommended limit of viscosity for nozzle application. Too-high viscosity causes the creation of liquid filaments instead of a spray at the nozzle outlet and increases fuel pump consumption [25]. In this research, the recommended limit of viscosity is 100 mm^2/s. Nevertheless, according to our experimental observations, the good-enough atomization of liquid fuel was observed for kinematic viscosity lower than 20 mm^2/s (calculated from dynamic viscosity and estimated density). At this value of viscosity (for FADR temperature in the range of 70 °C) and proper pressure, efficient atomization was observed at a nozzle diameter of 0.5 mm (see Table 3). Lezsovits and Könczöl [16] mentioned that the recommended nozzle viscosity for atomization of liquid fuels (i.e., animal fat and HFO) was in the range of 7–10 mm^2/s. Alonso et al. [12] reported the maximum viscosity at the nozzle in the range of 50–118 mm^2/s. A comparison of the kinematic viscosity of selected liquid fuels (i.e., HFO and fat-delivered fuels) as a function of temperature is presented in Figure 3. It can be noticed that HFOs have significantly higher values of kinematic viscosity; thus, this fuel should be heated up to a certain temperature (usually 100 °C) to obtain a proper value of viscosity. It is known that the viscosity (at 20 °C) of commercial liquid fuels (i.e., biodiesel, diesel, E15, and gasoline) was in the range of 0.79–8.34 mm^2/s [26]. Alonso et al. [12] noticed that the kinematic viscosity of animal by-products not intended for human consumption (ABNIHC) was 51.97 mm^2/s and 9.06 mm^2/s for 40 °C and 100 °C, respectively.

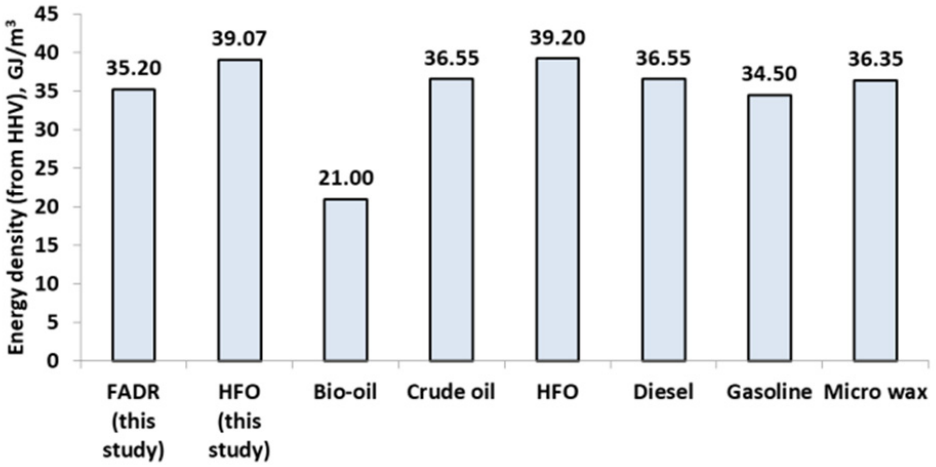

Figure 2. The comparison of energy density, GJ/m^3, based on the HHV, data from this study, and [22,27].

Table 2. Basic properties of the fatty acids distillation residues, FADR, and heavy fuel oil, HFO.

Parameter	FADR	HFO
Density (60 °C), kg/m^3	882	864
Ignition temperature (open vessel), °C	227	250
LHV, kJ/kg	36,619	42,251
HHV, kJ/kg	39,914	45,222
Energy density, $E_{d,\ LHV}$, GJ/m^3 (from LHV)	32.298	36.505
Energy density, $E_{d,\ HHV}$ GJ/m^3 (from HHV)	35.20	39.07
Ash content, w.%	0.28	0.36
C, w.%	76.6	86.1
H, w.%	12.45	13.61
N, w.%	0.85	0.56
S, w.%	0.16	0.62
Cl, w.%	<0.005%	<0.005%
Distillation beginning, °C	98	168
to 235 °C	1.9	2
235–270 °C	1	1.8
270–300 °C	3	2.4
300–330 °C	52.5	5.5
330–360 °C		35.9
Distillation residue, %	31.9	47.5
Distillation loses, %	9.7	4.9
Viscosity, Pa·s, at temperature		
30 °C	0.1954	
40 °C	0.0541	
50 °C		0.136
60 °C	0.0255	0.057
70 °C		0.034
80 °C	0.0142	0.0244
90 °C		0.0189
100 °C		0.0152

Table 3. The flow characteristic of FADR by nozzle, temperature of 70 °C.

Pressure	Flow Rate	Expected Input Power, kW	Visual Evaluation of Atomization
kPa	kg//h	kW	
		Nozzle 1 mm	
56	1.1	11	Droplets
67	1.3	13	Compact flow
82	4.9	50	Compact flow
112	11	112	Compact flow
150	17	173	Compact flow
165	19.5	198	Compact flow
168	20	203	Compact flow
195	off the scale		Compact flow
		Nozzle 0.5 mm	
385	7.4	75	Compact flow
429	8.2	83	Compact flow
470	9.3	95	Compact flow
502	9.9	101	Compact flow with spontaneous droplets
512	10.2	104	Fine droplets
528	10.3	105	Ultra-fine droplets and fog-like flow

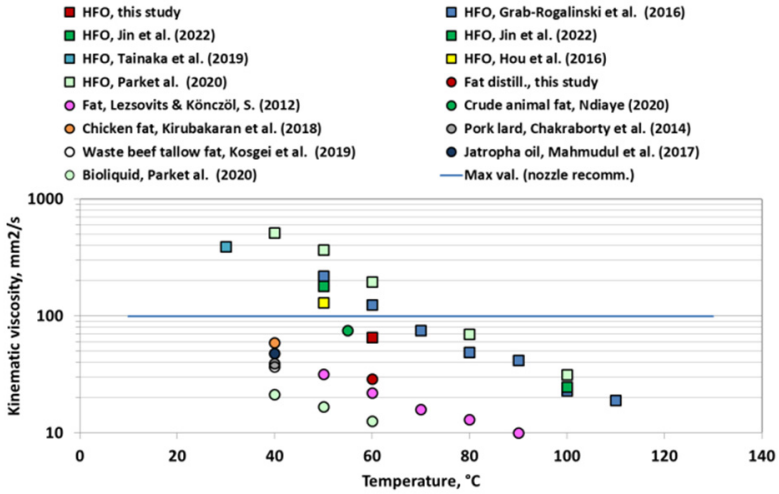

Figure 3. The comparison of kinematic viscosity of heavy fuel oil, HFO, and animal fats, data from [5,16,28–36].

The required viscosity in terms of temperature is directly related to the energy demand on the fuel transportation and the efficient atomization behind the nozzle spray. The specific heat capacity of animal fat is very close to the specific heat capacity of diesel fuel [37]. At a temperature of 293K and pressure of 0.1 MPa, the heat capacity of diesel is 1.9 kJ/kgK [38,39]. The average specific heat of crude oil is in a similar range of 2.2 kJ/kgK [40]. The properties of micro wax were taken from [22,41,42] (heat capacity [41,42] c_p at a level of 2.5 kJ/kgK). The specific heat of HFO was assumed on a similar level. The energy demand on fuel transportation has two specific parts: (a) the energy necessary to heat the fuel up to a certain level of enough viscosity; and (b) the energy related to the pressurization of the fuel before its introduction to the nozzle. It is assumed that the energy demand refers to the mass of fuel (i.e., kJ/kg); thus, the energy for fuel heating and fuel pressurization were calculated according to Equations (14) and (15), respectively:

$$E_{heat} = c_p\left(T_{fuel} - T_{room}\right),\ \text{kJ/kg} \tag{14}$$

$$E_{pressur} = \frac{p}{\rho},\ \text{kJ/kg} \tag{15}$$

The sum of E_{heat} and $E_{pressur}$ is defined as E_{total}.

When nominal fuel feed $\dot{m}_{nominal}$, kg/s at 100 kW_{th}, power is calculated from Equation (16)

$$\dot{m}_{100\text{kW}} = \frac{100}{LHV} \tag{16}$$

Then power loss, P_{loss}, kW is (Equation (17))

$$P_{loss} = \frac{\dot{m}_{100\text{kW}}}{\left(E_{heat} + E_{pressur}\right)} \tag{17}$$

The nominal feed of analyzed fuel at 100 kW_{th} power was in the range of 8.25–9.83 kg/h. Nominal fuel feed $\dot{m}_{nominal}$, in the case of FADR (i.e., 9.83 kg/h) was higher compared with the value for HFO (i.e., 8.52 kg/h). This was due to the lower calorific value of FADR (i.e., LHV 36619 kJ/kg) compared with HFO (i.e., LHV 42251 kJ/kg). It should be underscored that the assumption of nominal power at 100 kW_{th} is very useful, since the power loss is easily transformed into %. The results of energy and power loss due to the demands on fuel transportation and heating are presented in Figures 4 and 5. It can be noticed that in almost all cases the total energy demand varies in the range of 320–806 kJ/kg of combusted fuel, and the more significant component is from the pressurization demand

(i.e., in the range of 273–635 kJ/kg). This range is consistent with the values presented by Alonso et al. [12], who reported the required energy in the range of 180–540 kJ/kg of fuel feed (0.05–0.15 kWh/kg) depending on burner technology. In one case, the energy demand was significantly higher due to the higher value of the pressurization component. Namely, Bondrea et al. [17] reported the necessary pressure for atomization at the level of 14 bar. The lowest energy demand (i.e., E_{total} 320 kJ/kg) was observed by Lasek et al. during micro wax combustion [22]. Except for the Bondrea et al. [17] study, the power loss is less than 2% (i.e., in the range of 0.73–1.94%). It is less than 2 kW_{th} for the nominal input power of 100 kW_{th}. Except for the Bondrea et al. [17] study, the required pressure of fuel was in the range of 219–635 kPa. The flow characteristics of FADR by nozzle (diameter of 1 mm and 0.5 mm) are presented in Table 3. It is clear that in the case of this study, the nozzle with a diameter of 1 mm was not efficient due to the too-high value of flow rate, as well as the inefficient atomization quality. The good-enough parameters were obtained using a 0.5 mm nozzle. At a pressure of 528 kPa, the FADR flow rate was in the range of 10.3 kg/h, which is referred to as 105 kW of input power. Lezsovits and Könczöl [16] reported that the spray formation of animal fat was satisfactory at a pre-heating temperature of 60–95 °C; nevertheless, during the experimental run they kept the temperature at a level of 94–96 °C. Alonso et al. [9] recommended a higher pressure of fats after the pump (i.e., 10–30 bar); whereas, in the case of this study, it was 5.26 bar.

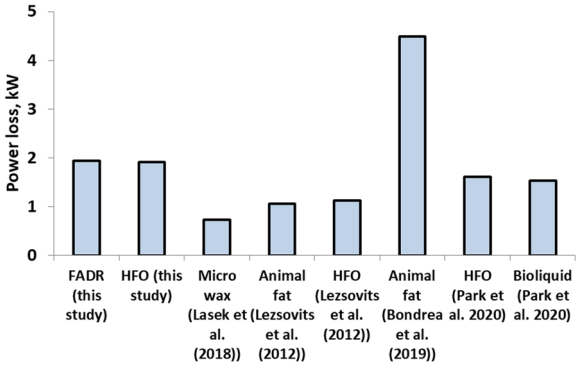

Figure 4. Power loss due to demands on fuel transportation and heating, data from [16,17,22,36], assumed nominal power 100 kW_{th}.

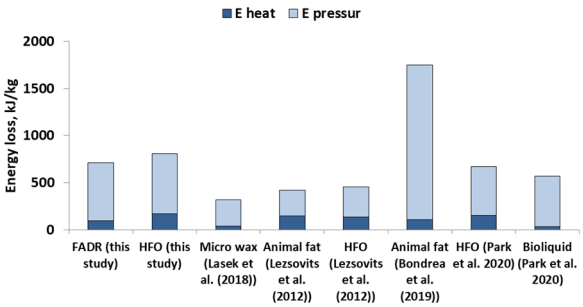

Figure 5. Energy per fuel mass loss due to demands on fuel transportation ($E_{pressur}$) and heating (E_{heat}), data from [16,17,22,36].

FADR has a significantly lower sulfur content, which is directly related to the lower SO_2 emission. Nitrogen content in FADR is higher (i.e., 0.85 w.%) compared with HFO (i.e., 0.56 w.%). It is known that nitrogen content in fuels influences NOx emission. This issue will be discussed in the Emissions section.

3.2. Combustion Test

The results of combustion performance in terms of temperature inside the combustion chamber, air flow rate, and fuel flow rate, as well as the liquid fuel overpressure behind the

pump, are presented in Table 4. The examples of time-dependent results are presented in Figures 6 and 7. The combustion of FADR and HFO was stable; nevertheless, during the initial period of liquid fuel combustion (i.e., 17:30) the flow rate of FADR was initially very high. After this period, the flow rate of FADR was stabilized and the temperature inside the combustion chamber was kept at a certain level of 1000 °C. The fraction of secondary air in the total sum of air was in the range of 20–22%.

Table 4. Main process parameters during combustion of FADR and HFO.

		FADR		HFO	
Parameter	Unit	Aver.	±		
The temperature in the chamber, top zone	°C	1028	15	1070	9
The temperature in the chamber, middle zone	°C	1006	15	985	2
The temperature in the chamber, bottom zone	°C	1007	9	890	2
The temperature in the chamber outlet (after heat exch.)	°C	748	6	550	3
Temperature of liquid fuel at burner inlet	°C	70	<1	110	<1
Primary air flow rate	Nm^3/h	105	1	70	1
Secondary air flow rate	Nm^3/h	30	<1	18	<1
Liquid fuel flow rate	kg/h	10.6	0.4	5.27	0.21
Liquid fuel overpressure behind the pump	kPa	542	8	549	4

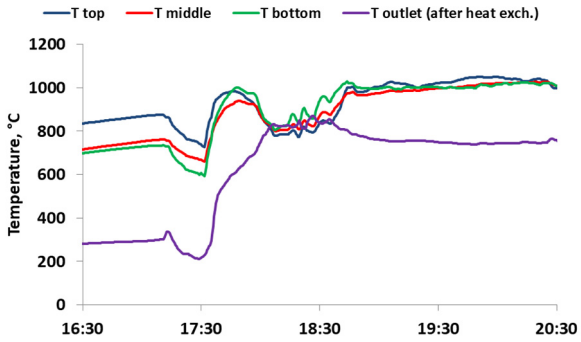

Figure 6. The temperature in the chamber, top zone, middle zone, bottom zone, and chamber outlet after heat exchanger as a function of time.

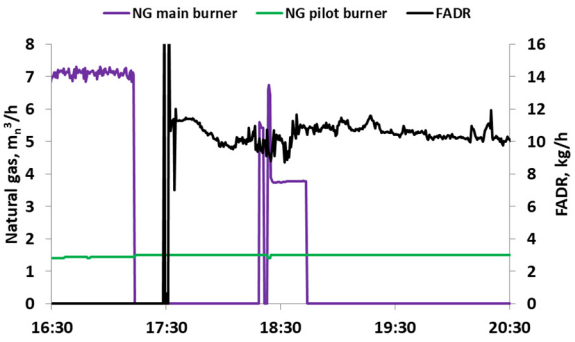

Figure 7. The flow rate of gaseous (natural gas, NG) and liquid (FADR) fuels as a function of time.

3.3. Emission

Figures 8–10 present the concentration of selected compounds in the flue gas as a function of time. The period of 16:30–16:45 represents the combustion of natural gas. At 17:30, the liquid fuel was introduced (please compare with Figure 7). In the starting period (ignition, flow stabilization), the emission of carbon monoxide and hydrocarbons was very high. After the unstable period, the emission came back to a stable level. This period was used to evaluate the average values of the emissions, presented in Table 5. The emission

was compared with the values obtained by other research groups. It should be underscored that the emission of SO_2 was significantly decreased, and the emission of NO_x was a little increased during the combustion of FADR. The lower emission of SO_2 was caused by the limitation of sulfur content in the fuel, which is a main parameter influencing SO_2 emission. A decrease in SO_2 (from 1180 ppm to 40 ppm) and NO_x (from 201 ppm to 126 ppm) due to a decrease in S- and N-fuel content was observed by Park et al. [43], who presented the CFD modeling and experimental results of HFO and bioliquid, BL (a blend of palm oil, its residue, and animal fat), combustion in a 400-MW_e power boiler. Fuel-N content in HFO and BL was 0.46 w.% and 0.19 w.%, respectively. Sulfur content in HFO and BL was 2.04 w.% and 0.04 w.%, respectively. A similar phenomenon was observed by Park et al. [44].

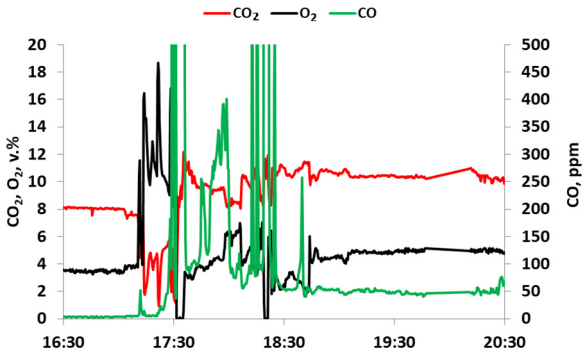

Figure 8. The concentration of CO_2, O_2, and CO in flue gas during the combustion of natural gas and FADR.

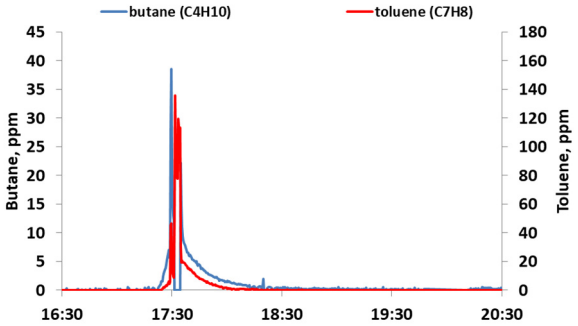

Figure 9. The emission of butane and toluene as a function of time during combustion of natural gas and FADR.

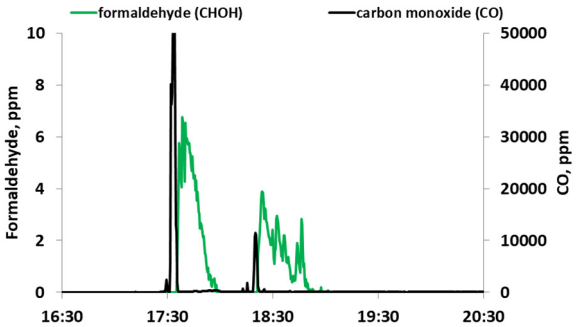

Figure 10. The emission of formaldehyde and carbon monoxide as a function of time during combustion of natural gas and FADR.

Apart from fuel NO, NO_x primarily originates from thermal NO and prompt NO [45]. The emission of NO_x during the combustion of liquid fuels is a complex process influenced by different factors. The difference in the NO_x emissions between non-food fat-type

fuels, NF1 and NF2, in investigations by Alonso et al. [9] was caused (inter alia) by the significant difference in N-content. Namely, N-content in NF1 and NF2 was 0.16 w.% and 0.05 w.%, respectively; nevertheless, during the combustion of liquid fuels, N-fuel content is not the only factor that influences NO_x emission. Some comparisons of the experimental results of liquid fuel combustion confirm that the increase in N-fuel content did not increase NO_x emission in all cases. For example, Lezsovits and Könczöl [16] noticed lower emission of NO_x during the combustion of animal fat (164 ppm referred to as 3 vol% O_2) compared with HFO combustion (295 ppm referred to as 3 vol% O_2), despite the higher N-content in animal fat (i.e., 0.35 w.%) compared with HFO (i.e., 0.3 w.%). Lehto and colleagues [46] explained that the total NO_x is a combination of thermal and fuel-bound nitrogen mechanisms. In some cases, lower flame temperature significantly reduces the emission of NO_x. Darbandi et al. [47] noticed that the emission of NOx during HFO combustion can be significantly influenced (in the range of 300–450 ppm) by the change in air distribution, swirl ratio of secondary air (0.5–1.4), mean droplet size (25–150 μm), and fuel injection velocity (20–120 m/s). Among the other crucial effects, Rebola and Costa [48] listed the atomizing air-to-fuel mass ratio (AFR), secondary air swirl number (Ss), air staging, burning using methane and propane as secondary fuels, and fuel atomization using mixtures of air and methane. Bazooyar et al. [49] concluded that an "increase in the combustion pressure leads to more uniform combustion (better vaporization and propagation of fuel in the chamber) and the formation of high-quality sprays (smaller droplet size, deep penetration of sprays in chambers). This contributes to high local temperatures and disappearance of fuel local rich zones". The study by Bazooyar et al. [49] included the combustion of biodiesel and petrodiesel in utility power plant boilers. They noticed that the contribution of the percent of thermal and prompt NO into total NO varied by a wide range. For example, the contribution of thermal NO changed in the range of 16–73% when combustion pressure changed in the range of 8–22 bar. Wu et al. [50] noticed significantly higher NO_x emission (473 ppm, 3% O_2) during the combustion of HFO using a 1.4 MW_{th} experimental rig. The experimental setup included a regenerator–burner system with highly preheated combustion air at 1200 °C and a furnace temperature at the level of 1300 °C. Thus, despite moderate N-content (i.e., N 0.21 w.%) and due to the thermal-NO_x mechanism, the NO_x emission was higher compared with the combustion of HFO at a similar or higher level. Figure 11 presents the comparison of the NO_x emission as a function of N-fuel content. The data were divided into two main groups: heavy fuel oils, HFO, and bio-liquid fuels. The relationship between the emission of NO_x and nitrogen content in combustion fuels is a complex issue. An overall conclusion from the data collected in Table 5 is that the concentration of NO during the combustion of liquid fuels is in the range of 31–432 ppm (ref. to 3 v.% O_2). Increase in NO_x emission was also observed when diesel was substituted by biodiesel in diesel engines [51].

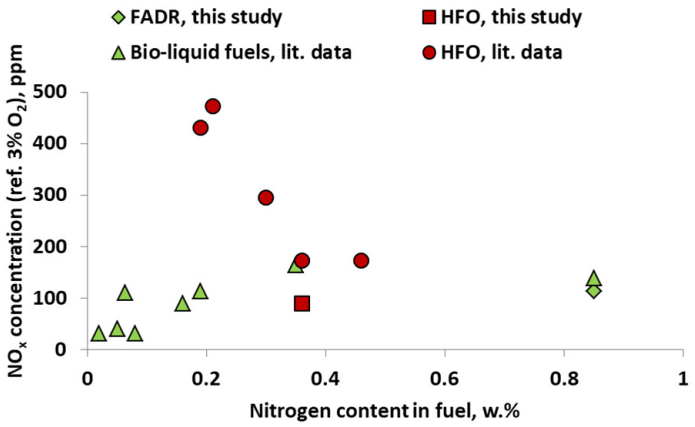

Figure 11. The emission of NOx in the function of N-fuel content, data from [9,12,16,18,43,47,50].

Table 5. Comparison of the emission of gaseous pollutants during the combustion of heavy fuel oil and bio-liquid fuels.

Fuel	Type and Scale of the Facility	Emissions	O_2 in Gases, %	Emissions (Calculated on 3% O_2)	Ref.
FADR	150 kW tech-scale combustion chamber	CO 55 ppm; NO 98 ppm; SO_2 < 1 ppm	5	CO 64 ppm; NO 114 ppm; SO_2 < 1 ppm	This study
HFO	150 kW tech-scale combustion chamber	CO 26 ppm; NO 68 ppm; SO_2 133 ppm	7.9	CO 35 ppm; NO 90 ppm; SO_2 176 ppm	This study
Blend of diesel (60 w.%) and FF (40 w.%)	26.7 kW boiler	CO 198 ppm; NO 27 ppm	5.4	CO 228 ppm; NO 31 ppm	[9]
Blend of diesel (60 w.%) and NF1 (40 w.%)	26.7 kW boiler	CO 634 ppm; NO 98 ppm	5.1	CO 718 ppm; NO 111 ppm	[9]
Blend of diesel (60 w.%) and NF2 (40 w.%)	26.7 kW boiler	CO 62 ppm; NO 28 ppm	4.9	CO 69 ppm; NO 31 ppm	[9]
AF	rotary cup type burner in 4 MW_{th} boilers.	CO 1 ppm; NO 124 ppm	7.4	CO 1 ppm; NO 164 ppm	[16]
BL	400-MW_e power boiler	NO 126 ppm, SO_2 40 ppm	1	NO 113 ppm, SO_2 36 ppm	[43]
ABNIHC category 1	technical-scale combustion chamber	CO 50 ppm; NO 56 ppm	9.8	CO 80 ppm; NO 90 ppm	[12]
ABNIHC category 2	technical-scale combustion chamber	CO 32 ppm; NO 22 ppm	11	CO 58 ppm; NO 40 ppm	[12]
FADR	4.5 MW_{th} nominal capacity boiler	CO 4 ppm; NO 118 ppm; SO_2 16 ppm	5	CO 5 ppm; NO 139 ppm; SO_2 18 ppm	[18]
HFO	4.5 MWth nominal capacity boiler	CO 6 ppm; NO 148 ppm; SO_2 288 ppm	5	CO 7 ppm; NO 173 ppm; SO_2 337 ppm	[18]
HFO	1.4 MWth experimental rig. The heavy-fuel-oil-fired regenerator-burner system with the 1200 °C highly preheated combustion air, furnace temp 1300 °C	NO 394 ppm	6	NO 473 ppm	[50]
HFO	325 MW boiler	NO 398 ppm	4.4	NO 432 ppm	[47]
HFO	400-MW_e power boiler	NO 201 ppm, SO_2 1180 ppm	0.125	NO 173 ppm, SO_2 1017 ppm	[43]
HFO	rotary cup type burner in 4 MW_{th} boilers.	CO 36 ppm; NO 279 ppm	4	CO 38 ppm; NO 295 ppm	[16]

FADR-fatty acids distillation residues, HFO-heavy fuel oil, FF-food fat, NF1-non-food fat type 1, NF2-non-food fat type 2, BL-a blend of palm oil, its residue, and animal fat, ABNIHC-animal by-products not intended for human consumption, AF-animal fat.

The emission of polycyclic aromatic hydrocarbons (PAHs) during the combustion of HFO, FADR, and micro wax [22] is presented in Table 6. It was observed that in both cases of alternative fuels (i.e., FADR and micro wax), the total emission of PAHs (355.5 $\mu g/m^3_n$ and 198.5 $\mu g/m^3_n$) was lower compared with the value in the case of HFO combustion (i.e., 810.4 $\mu g/m^3_n$). Lasek et al. [22] concluded that during the combustion of HFO, the average value of PAH emission was 488 $\mu g/m^3_n$; nevertheless, the highest emission was in the range of 3530 $\mu g/m^3_n$. PAHs are created using the incomplete combustion of organic material, and the main factors influencing the value of emission are the type of fuel and additive, air pollution control devices, combustion control, and performance (air distribution, temperature, residence time, etc.). During the combustion of FADR, the highest values of emission (i.e., in the range of 50 $\mu g/m^3_n$) were observed for acenaphthylene, acenaphthene, fluorine, phenanthrene, and anthracene. In the case of fluoranthene, pyrene, and benzo (b + k) fluoranthene, the emission was in the range of 20–30 $\mu g/m^3_n$. The emission of the rest of the compounds was less than 5 $\mu g/m^3_n$. It is also worth underscoring the low emission of benzo(a)pyrene during the combustion of FADR (i.e., 0.73 $\mu g/m^3_n$). The emission of benzo(a)pyrene during the combustion of HFO was significantly higher (i.e., 30.6 $\mu g/m^3_n$). The reduction in PAH emissions from diesel engines was observed when diesel was substituted with biodiesel [51].

Table 6. Concentration ($\mu g/m^3_n$) of polycyclic aromatic hydrocarbons (PAHs) in dry flue gas (ref to 3% O_2).

Compound	Emission		
	HFO	**FADR**	**Micro Wax Data from [22]**
naphthalene	8.5	10.9	2.1
acenaphthylene	10.2	57.4	2.0
acenaphthene	12.6	49.8	1.0
fluorene	14	48.2	5.0
phenanthrene	72.2	53.5	12.2
anthracene	34.2	50.6	1.7
fluoranthene	75.4	29.2	9.7
pyrene	81.4	26.2	4.8
benzo(a)anthracene	15.1	3.5	1.0
chrysene	9.5	1.4	13.3
benzo (b + k) fluoranthene	30.5	20.7	110.6
benzo(e)pyrene	290.3	0.55	1.0
benzo(a)pyrene	30.6	0.73	22.7
perylene	11.5	2.8	8.2
bibenzo(a, h) anthracene + indeno (1,2,3) pyrene	98.4	0.02	1.8
benzo(g, h, i)perylene	16	0.04	1.4
Total PAHs	810.4	355.5	198.5

4. Conclusions

The properties and combustion performance of heavy fuel oil, HFO, and the products of the fatty acids distillation residues, FADR, were analyzed in this study. It was observed that FADR can be considered as a substitute for HFO due to the similarity in calorific as well as physical properties (density and viscosity). It is worth underscoring that FADR includes significantly lower sulphur, which is directly related to the lower SO_2 emission. On the other hand, FADR calorific value (LHV 36,619 kJ/kg) is lower compared with the HFO (LHV 42,251 kJ/kg); nevertheless, due to the higher density of FADR (i.e., 882 kg/m^3 at 60 °C) compared with HFO (i.e., 864 kg/m^3 at 60 °C), the energy density of FADR (i.e., 32.298 GJ/m^3 (from LHV)) is 88.5% of the value for HFO (i.e., 36.505 GJ/m^3 (from LHV)). FADR is characterized by the lower energy demand on heating up fuel and pressurization (i.e., 710 kJ/kg) compared with the value for HFO (i.e., 806 kJ/kg). It was caused by the required lower pressure after the fuel pump, as well as lower temperature to obtain the required viscosity. The combustion performance of HFO and FADR was stable. The

emission of NO during the combustion of FADR (i.e., 114 ppm at 3% O_2) was slightly higher compared with the emission during the combustion of HFO (i.e., 90 ppm at 3% O_2). Finally, lower emission of PAHs was observed during the combustion of FADR (i.e., 355.5 $\mu g/m^3_n$) compared with the emission of HFO (i.e., 810.4 emission $\mu g/m^3_n$). Thus, due to the many benefits related to the FADR application, future work should contain the analysis of FADR utilization as a fuel in energy systems.

Author Contributions: Conceptualization, J.L., K.G., A.C., Y.-H.L. and C.-W.H.; methodology, J.L., K.G., A.C., Y.-H.L. and C.-W.H.; investigation, J.L. and K.G.; data curation, J.L.; writing—original draft preparation, J.L.; writing—review and editing, J.L.; supervision, J.L. and Y.-H.L., project administration, J.L., K.G. and A.C.; funding acquisition, J.L., K.G., A.C., Y.-H.L. and C.-W.H. All authors have read and agreed to the published version of the manuscript.

Funding: This research was funded by a grant from the Ministry of Education and Science, the Republic of Poland. Grant title and number: "Utrzymanie potencjału badawczego ZTE"; No. ITPE 11.23.017.

Institutional Review Board Statement: Not applicable.

Informed Consent Statement: Not applicable.

Data Availability Statement: The data presented in this study are available on request from the corresponding author. The data are not publicly available due to privacy.

Acknowledgments: Edyta Misztal is acknowledged for support in the uncertainty analysis.

Conflicts of Interest: The authors declare no conflict of interest.

References

1. Alrashidi, A.M.R.N.; Adam, N.M.; Bin Mohd Ariffin, M.K.A.; Fnyees, A.; Alajmi, A.; Naser, A.; Abdul Aziz, H. Impact of Plasma Combustion Technology on Micro Gas Turbines Using Biodiesel Fuels. *Appl. Sci.* **2022**, *12*, 4321. [CrossRef]
2. Lee, C.Y.; Sun, W.C.; Li, Y.H. Biodiesel Economic Evaluation and Biomass Planting Allocation Optimization in Global Supply Chain. *IEEE Trans. Eng. Manag.* **2022**, *69*, 602–615. [CrossRef]
3. Chen, G.-B.; Li, Y.-H.; Lan, C.-H.; Lin, H.-T.; Chao, Y.-C. Micro-explosion and burning characteristics of a single droplet of pyrolytic oil from castor seeds. *Appl. Therm. Eng.* **2017**, *114*, 1053–1063. [CrossRef]
4. Kupczyk, A.; Mączyńska, J.; Redlarski, G.; Tucki, K.; Bączyk, A.; Rutkowski, D. Selected Aspects of Biofuels Market and the Electromobility Development in Poland: Current Trends and Forecasting Changes. *Appl. Sci.* **2019**, *9*, 254. [CrossRef]
5. Ndiaye, M.; Arhaliass, A.; Legrand, J.; Roelens, G.; Kerihuel, A. Reuse of waste animal fat in biodiesel: Biorefining heavily-degraded contaminant-rich waste animal fat and formulation as diesel fuel additive. *Renew. Energy* **2020**, *145*, 1073–1079. [CrossRef]
6. Rosson, E.; Sgarbossa, P.; Pedrielli, F.; Mozzon, M.; Bertani, R. Bioliquids from raw waste animal fats: An alternative renewable energy source. *Biomass Convers. Biorefin.* **2021**, *11*, 1475–1490. [CrossRef]
7. Toldrá-Reig, F.; Mora, L.; Toldrá, F. Trends in Biodiesel Production from Animal Fat Waste. *Appl. Sci.* **2020**, *10*, 3644. [CrossRef]
8. Borychowska, H.; Dziejowska, I.; Orżanowska, A.; Rafa, W.; Wróblewska, A. *Statistical Yearbook of Agriculture*; Statistics: Warsaw, Poland, 2022.
9. Alonso, J.F.S.J.; Arribas, I.G.; Miñambre, S.A. Study of combustion in residential oil burning equipment of animal by-products and derived products not intended for human consumption. *Int. J. Energy Environ. Eng.* **2013**, *4*, 31. [CrossRef]
10. Brahma, S.; Nath, B.; Basumatary, B.; Das, B.; Saikia, P.; Patir, K.; Basumatary, S. Biodiesel production from mixed oils: A sustainable approach towards industrial biofuel production. *Chem. Eng. J. Adv.* **2022**, *10*, 100284. [CrossRef]
11. Xiu, S.; Shahbazi, A. Bio-oil production and upgrading research: A review. *Renew. Sustain. Energy Rev.* **2012**, *16*, 4406–4414. [CrossRef]
12. Alonso, J.S.J.; Romero-Ávila, C.; Hernández, L.S.J.; Awf, A.-K. Characterising biofuels and selecting the most appropriate burner for their combustion. *Fuel Process. Technol.* **2012**, *103*, 39–44. [CrossRef]
13. Tsui, T.-H.; Wong, J.W. A critical review: Emerging bioeconomy and waste-to-energy technologies for sustainable municipal solid waste management. *Waste Dispos. Sustain. Energy* **2019**, *1*, 151–167. [CrossRef]
14. Fakudze, S.; Wei, Y.; Shang, Q.; Ma, R.; Li, Y.H.; Chen, J.; Zhou, P.; Han, J.; Liu, C. Single-pot upgrading of run-of-mine coal and rice straw via Taguchi-optimized hydrothermal treatment: Fuel properties and synergistic effects. *Energy* **2021**, *236*, 121482. [CrossRef]
15. Li, Y.H.; Kuo, W.C. The study of optimal parameters of oxygen-enriched combustion in fluidized bed with optimal torrefied woody waste. *Int. J. Energy Res.* **2020**, *44*, 7416–7434. [CrossRef]
16. Lezsovits, F.; Könczöl, S. Animal-fat investigation and combustion test. *J. Therm. Anal. Calorim.* **2012**, *107*, 271–278. [CrossRef]

17. Bondrea, D.A.; Mihaescu, L.; Lazaroiu, G.; Pisa, I.; Negreanu, G. Researches on the mixture limits of animal fats with liquid hydrocarbons for combustion at industrial level. In *E3S Web of Conferences*; EDP Sciences: Les Ulis, France, 2019; p. 02001.
18. Wasielewski, R.; Głód, K. Emission results of combustion process of fatty acids distillation residue in an oil boiler–comparison to heavy fuel oil. *Sci. Rev. Eng. Environ. Sci.* **2020**, *2020*, 62–71. [CrossRef]
19. Lazaroiu, G.; Mihaescu, L.; Negreanu, G.; Pana, C.; Pisa, I.; Cernat, A.; Ciupageanu, D.-A. Experimental investigations of innovative biomass energy harnessing solutions. *Energies* **2018**, *11*, 3469. [CrossRef]
20. Lasek, J.A.; Matuszek, K.; Hrycko, P.; Piechaczek, M. Adaptation of hard coal with high sinterability for solid fuel boilers in residential heating systems. *Fuel* **2018**, *215*, 239–248. [CrossRef]
21. Biernat, K. Criteria for the Quality Assessment of Engine Fuels in Storage and Operating Conditions. In *Storage Stability of Fuels*; IntechOpen: London, UK, 2015.
22. Lasek, J.; Hrycko, P.; Wasielewski, R.; Kopczyński, M.; Bodora, K.; Kaczmarzyk, G.; Adamczyk, M. Combustion of micro wax from polyethylene pyrolysis. *Combust. Sci. Technol.* **2018**, *190*, 1246–1258. [CrossRef]
23. Lasek, J.; Matuszek, K.; Stelmach, S.; Sobolewski, A.; Hrycko, P. Smokeless Fuel for Residential Heating as a Remedy for Air Pollution: Laboratory and Pilot-Scale Operational Investigations. *Energy Fuels* **2019**, *33*, 11757–11767. [CrossRef]
24. Lasek, J.A.; Kopczyński, M.; Janusz, M.; Iluk, A.; Zuwała, J. Combustion properties of torrefied biomass obtained from flue gas-enhanced reactor. *Energy* **2017**, *119*, 362–368. [CrossRef]
25. Eryilmaz, T.; Yesilyurt, M.K. Influence of blending ratio on the physicochemical properties of safflower oil methyl ester-safflower oil, safflower oil methyl ester-diesel and safflower oil-diesel. *Renew. Energy* **2016**, *95*, 233–247. [CrossRef]
26. Jiang, G.; Zhang, Y.; Wen, H.; Xiao, G. Study of the generated density of cavitation inside diesel nozzle using different fuels and nozzles. *Energy Convers. Manag.* **2015**, *103*, 208–217. [CrossRef]
27. Chen, D.; Zhou, J.; Zhang, Q.; Zhu, X. Evaluation methods and research progresses in bio-oil storage stability. *Renew. Sustain. Energy Rev.* **2014**, *40*, 69–79. [CrossRef]
28. Grab-Rogalinski, K.; Szwaja, S. The combustion properties analysis of various liquid fuels based on crude oil and renewables. In *IOP Conference Series: Materials Science and Engineering*; IOP Publishing: Bristol, UK, 2016; p. 012066.
29. Jin, C.; Sun, T.; Ampah, J.D.; Liu, X.; Geng, Z.; Afrane, S.; Yusuf, A.A.; Liu, H. Comparative study on synthetic and biological surfactants' role in phase behavior and fuel properties of marine heavy fuel oil-low carbon alcohol blends under different temperatures. *Renew. Energy* **2022**, *195*, 841–852. [CrossRef]
30. Tainaka, K.; Fan, Y.; Hashimoto, N.; Nishida, H. Effects of blending crude Jatropha oil and heavy fuel oil on the soot behavior of a steam atomizing burner. *Renew. Energy* **2019**, *136*, 358–364. [CrossRef]
31. Hou, S.-S.; Huang, W.-C.; Rizal, F.M.; Lin, T.-H. Co-firing of fast pyrolysis bio-oil and heavy fuel oil in a 300-kWth furnace. *Appl. Sci.* **2016**, *6*, 326. [CrossRef]
32. Kirubakaran, M.; Selvan, V.A.M. A comprehensive review of low cost biodiesel production from waste chicken fat. *Renew. Sustain. Energy Rev.* **2018**, *82*, 390–401. [CrossRef]
33. Kosgei, C.; Inambao, F.L. A Comprehensive Review of Low-Cost Biodiesel Production from Waste Beef Tallow. *Int. J. Mech. Eng. Technol.* **2019**, *10*, 285–305.
34. Chakraborty, R.; Gupta, A.K.; Chowdhury, R. Conversion of slaughterhouse and poultry farm animal fats and wastes to biodiesel: Parametric sensitivity and fuel quality assessment. *Renew. Sustain. Energy Rev.* **2014**, *29*, 120–134. [CrossRef]
35. Mahmudul, H.; Hagos, F.; Mamat, R.; Adam, A.A.; Ishak, W.; Alenezi, R. Production, characterization and performance of biodiesel as an alternative fuel in diesel engines—A review. *Renew. Sustain. Energy Rev.* **2017**, *72*, 497–509. [CrossRef]
36. Park, H.Y.; Han, K.; Kim, H.H.; Park, S.; Jang, J.; Yu, G.S.; Ko, J.H. Comparisons of combustion characteristics between bioliquid and heavy fuel oil combustion in a 0.7 MWth pilot furnace and a 75 MWe utility boiler. *Energy* **2020**, *192*, 116557. [CrossRef]
37. Geller, D.P.; Adams, T.T.; Goodrum, J.W.; Pendergrass, J. Storage stability of poultry fat and diesel fuel mixtures: Specific gravity and viscosity. *Fuel* **2008**, *87*, 92–102. [CrossRef]
38. Dzida, M.; Prusakiewicz, P. The effect of temperature and pressure on the physicochemical properties of petroleum diesel oil and biodiesel fuel. *Fuel* **2008**, *87*, 1941–1948. [CrossRef]
39. Safarov, J.; Ashurova, U.; Ahmadov, B.; Abdullayev, E.; Shahverdiyev, A.; Hassel, E. Thermophysical properties of Diesel fuel over a wide range of temperatures and pressures. *Fuel* **2018**, *216*, 870–889. [CrossRef]
40. Ismail, I.; Mulyanto, A.T.; Rahman, R.A. Development of free water knock-out tank by using internal heat exchanger for heavy crude oil. *EUREKA Phys. Eng.* **2022**, *4*, 77–85. [CrossRef]
41. Cao, J.; Liu, L.; Liu, C.; He, C. Phase transition mechanisms of paraffin in waxy crude oil in the absence and presence of pour point depressant. *J. Mol. Liq.* **2022**, *345*, 116989. [CrossRef]
42. Ukrainczyk, N.; Kurajica, S.; Šipušić, J. Thermophysical comparison of five commercial paraffin waxes as latent heat storage materials. *Chem. Biochem. Eng. Q.* **2010**, *24*, 129–137.
43. Park, J.K.; Park, S.; Ryu, C.; Baek, S.H.; Kim, Y.J.; Park, H.Y. CFD analysis on bioliquid co-firing with heavy fuel oil in a 400MWe power plant with a wall-firing boiler. *Appl. Therm. Eng.* **2017**, *124*, 1247–1256. [CrossRef]
44. Park, J.-K.; Park, S.; Kim, M.; Ryu, C.; Baek, S.H.; Kim, Y.J.; Kim, H.H.; Park, H.Y. CFD analysis of combustion characteristics for fuel switching to bioliquid in oil-fired power plant. *Fuel* **2015**, *159*, 324–333. [CrossRef]
45. Li, Y.-H.; Pangestu, S.; Purwanto, A.; Chen, C.-T. Synergetic combustion behavior of aluminum and coal addition in hybrid iron-methane-air premixed flames. *Combust. Flame* **2021**, *228*, 364–374. [CrossRef]

46. Lehto, J.; Oasmaa, A.; Solantausta, Y.; Kytö, M.; Chiaramonti, D. Review of fuel oil quality and combustion of fast pyrolysis bio-oils from lignocellulosic biomass. *Appl. Energy* **2014**, *116*, 178–190. [CrossRef]
47. Darbandi, M.; Fatin, A.; Bordbar, H. Numerical study on NOx reduction in a large-scale heavy fuel oil-fired boiler using suitable burner adjustments. *Energy* **2020**, *199*, 117371. [CrossRef]
48. Rebola, A.; Costa, M. Simultaneous reduction of NOx and particulate emissionsfrom heavy fuel oil-fired furnaces. *Proc. Combust. Inst.* **2002**, *29*, 2243–2250. [CrossRef]
49. Bazooyar, B.; Hashemabadi, S.H.; Shariati, A. NOX formation of biodiesel in utility power plant boilers; Part B. Comparison of NO between biodiesel and petrodiesel. *Fuel* **2016**, *182*, 323–332. [CrossRef]
50. Wu, S.-R.; Chang, W.-C.; Chiao, J. Low NOx heavy fuel oil combustion with high temperature air. *Fuel* **2007**, *86*, 820–828. [CrossRef]
51. Wu, G.; Ge, J.C.; Choi, N.J. A Comprehensive Review of the Application Characteristics of Biodiesel Blends in Diesel Engines. *Appl. Sci.* **2020**, *10*, 8015. [CrossRef]